MDPI

Article

Combinatorial Synthesis of AlTiN Thin Films

Ferrine Gianne G. Reyes, Jason P. Licerio, Aian B. Ontoria and Magdaleno R. Vasquez, Jr. *

Department of Mining, Metallurgical and Materials Engineering, College of Engineering,
University of the Philippines Diliman, Quezon City 1101, Philippines
* Correspondence: mrvasquez2@up.edu.ph

Abstract: Nitrides of aluminum (Al) and titanium (Ti) mixtures have long been studied and used as commercial coatings because of their high hardness and high oxidation resistance due to the formation of an alumina layer on the coating surface. To fully understand the contribution of Al and Ti to the properties of the film, a combinatorial deposition approach was employed using half-disk targets. Film growth was carried out using a magnetron sputtering system powered by a 13.56 MHz radio frequency power supply with varying argon (Ar) and nitrogen (N_2) gas ratios. Depending on the location of the substrate relative to the target, atomic percent gradients of 0.60–0.70 Al and 0.30–0.40 Ti across the substrate surface were obtained from energy dispersive X-ray spectral analysis. X-ray diffraction peaks at 43.59°, 74.71° (face-centered cubic), and 50.60° (wurtzite) confirmed the presence of aluminum titanium nitride (AlTiN) mixtures, with an increasing amount of wurtzite phase at higher Al concentrations. For all samples, cauliflower-like nanograins were obtained and samples of the 80:20 Ar:N_2 gas pressure ratio showed the smallest grain size among the three gas ratio combinations. The 80:20 Ar:N_2 films revealed a relatively high hardness compared to the other gas ratios. All thin films exhibited good adhesion to 304 stainless steel substrates.

Keywords: thin films; AlTiN; combinatorial sputtering

1. Introduction

Recent advancements in hard coating synthesis have been made due to the demand for more wear-resistant tools for precision cutting and machining in manufacturing processes. As the manufacturing industry continues to grow and become more competitive, so does the need for better cutting tools, especially those applicable to higher operating temperatures [1]. Among the thin films used as hard coatings, aluminum titanium nitride (AlTiN) films have gained attention due to their high hardness values greater than 30 GPa [2–4] and their improved resistance to oxidation at high operating temperatures [5,6]. AlTiN possesses a mixture of wurtzite aluminum nitride (AlN) and cubic titanium nitride (TiN) structures, the latter contributing to improving the mechanical properties of the film. At high temperatures, AlTiN can form alumina (Al_2O_3), which further protects the substrate [7].

AlTiN thin films are commonly grown using several physical vapor deposition methods [4], such as arc evaporation [3,8], ion plating [6,9], and sputtering deposition processes [2,4]. In forming ternary thin films, one must consider the sputtering yield of the target atoms, which is the ratio between the number of ejected atoms from the target and the number of incident bombarding particles. In addition to the effect of the incident energy of the ions, the sputtering yield is also affected by the masses of the target atoms and incident ions [10]. Thus, by controlling the number of particles sputtered from a composite target, the stoichiometry of the deposited film can also be controlled.

The growth of AlTiN films is generally performed using Al and Ti targets and nitrogen (N_2) as the reactive gas with argon (Ar) as the background gas. The composition of the deposited thin film is generally determined based on the amounts of sputtered Al and Ti as well as the Ar:N_2 ratio. However, most AlTiN film synthesis has been performed only by

varying the Ar:N_2 gas ratios due to the limitations of current magnetron systems that have a single target mount. To allow high-throughput screening of the synthesized thin films with fewer runs, a combinatorial approach can be used, in which the sputtering system will have two different targets. Each target has its own sputtering gun, sometimes combining RF and DC sputtering [11,12], or even a combination of magnetron sputtering and arc deposition [3]. This will allow the production of a compositional gradient depending on the working distance of the lined-up substrates to the two targets. The combinatorial approach to sputter deposition has been applied on several thin film material systems. For instance, Hsu et al. [13] used the combinatorial approach to study high entropy nitrides and establish composition, structure, and mechanical property relationships. Bikowski et al. [14] used a combinatorial reactive sputtering approach to design metastable alloys and correlate them with theoretical calculations. A co-sputtering technique employed by Greenaway et al. [15] produced nitride semiconductors with varying compositions. Han et al. [16] studied the effect of the Ti-Al distribution on the mechanical properties of Ti-Al films and obtained maximum hardness from the Ti_3Al intermetallic as per nanoindentation test. Li et al. [17] also performed an optimization study of Al-Ti-N using two separate full targets of pure Ti and pure Al mounted at an angle of 45° relative to the substrate. A variation of $Ti_{0.82}Al_{0.18}N$ to $Ti_{0.12}Al_{0.88}N$ was reported after post-annealing, and a $Ti_{1-x}Al_xN$ film composition of x = 0.57 and 0.65 exhibited maximum wear resistance and minimum friction coefficient from the wear and friction test. Current combinatorial sputtering studies have used magnetron systems with two target mounts; hence, the feasibility of using half-disk targets in a single-target magnetron sputtering system for combinatorial thin-film synthesis is yet to be explored.

In this work, AlTiN films with varying Al and Ti content were combinatorially synthesized on 304 stainless steel (SS) substrates using a half-disk Al target and a half-disk Ti target. In addition, partial pressure ratios of Ar:N_2 were also varied. The compositional gradient of Ti-Al was obtained together with the elemental profiles and was correlated with the surface morphology and hardness.

2. Materials and Methods

2.1. Deposition of AlTiN Thin Films

Two-inch-diameter semicircular disk Ti (99.95%) and Al (99.95%) targets were purchased from Singapore Advantec and mounted on the target holder. Behind the target holder is an annular permanent magnet that realizes a magnetron configuration. Five 1 cm × 1 cm 304 SS substrates were mounted on a grounded substrate stage 10 cm from the targets. The substrates were arranged in a straight line, as shown in Figure 1. Substrate 1 is on the Ti-rich side, while substrate 5 is on the Al-rich side. Before deposition, to remove organic and inorganic debris from the surface, the substrates were ultrasonically cleaned for 10 min each in sequential acetone, ethanol, and deionized water baths using a Branson 1800 ultrasonicator (Branson, MO, USA). Subsequently, the substrates were blow-dried using compressed dry air.

After placing the pre-cleaned substrates on the substrate stage, the vacuum chamber was evacuated to a base pressure of around 10^{-3} Pa. The target was cleaned via pre-sputtering using ultra-high-purity (99.999%) Ar, after which both Ar and N_2 gases were introduced into the chamber in a predetermined partial pressure ratio. The total working pressure was maintained at 0.7 Pa. Plasma was excited using a 13.56 MHz radio frequency (RF) power source. Throughout the deposition, the substrate was not heated and no substrate bias was applied. Table 1 lists the parameters used in this study.

2.2. Characterization

Scanning electron microscopy (SEM) images were obtained using the Hitachi 8230 (Tokyo, Japan). SEM was used to investigate the surface microstructure of the thin films. Film thicknesses for different gas ratios and positions were measured using an Olympus LEXT (Tokyo, Japan) high-resolution laser scanning microscope, averaged from three

random spots. Energy-dispersive X-ray spectroscopy (EDX) using elemental linear scanning analysis was used to obtain the atomic percentage of the thin film across the surface. Line scans were obtained by taking SEM micrographs at a magnification of 25× and obtaining the average atomic percentage of the examined element for each image. X-ray diffraction (XRD) using a PANalytical Xpert PRO diffractometer was used to obtain information about the phase and crystallinity of the thin films. Bragg–Bentano analysis using Cu Kα radiation (λ = 1.54 Å) was used to identify the compound formed. Microhardness testing was performed for the center-position samples at gas ratios using the Shimadzu DUH-211S (Taguig, Philippines) dynamic ultra microhardness tester. Three points with a fixed depth of 0.5 µm per sample were indented at a loading speed of 3.3310 mN/s using a Vickers indenter with a diamond square-based pyramid, whose opposite sides meet at the apex at an angle of 136°. A qualitative adhesion test was performed alongside the dynamic microhardness test to check whether the thin film adheres to the stainless steel surface. The presence of cracking or delamination during indentation was observed and served as a basis for determining whether the thin film adheres well to the surface or not.

Table 1. Parameters used during the deposition of the thin films.

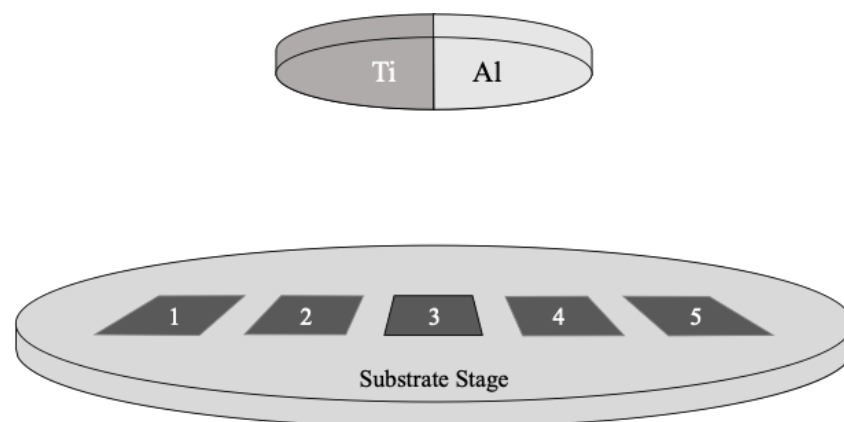| Parameter	Setting
RF power (W)	100
Deposition time (h)	3
Base pressure (Pa)	$\sim 10^{-3}$
Working pressure (Pa)	0.7
Gas admixture (Ar:N_2)	90:10, 80:20, 70:30

Figure 1. Schematic representation of the substrate positions (1, 2, 3, 4, and 5) relative to the half-disk targets, Ti and Al.

3. Results

3.1. Morphology

Images of the film surface are shown in Figure 2. Different deposition conditions reveal differences in the clustering density of the grains. Cauliflower-like morphologies were observed, with grain size increasing as samples were placed far from the target center as shown in Table 2.

Table 2. Average grain sizes of AlTiN thin films deposited at 90:10, 80:20, and 70:30 Ar:N_2 gas ratios.

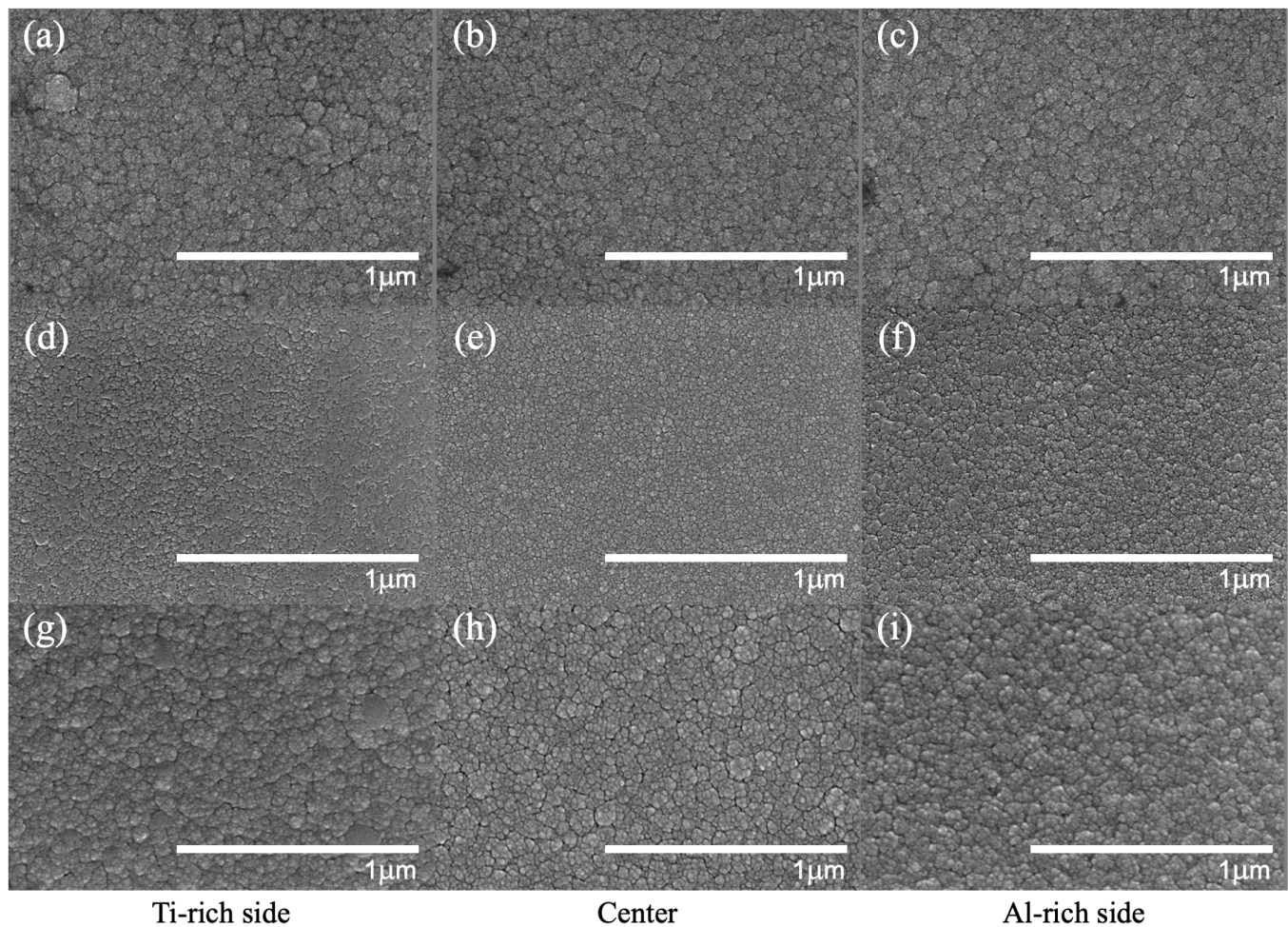| Ar:N_2 Ratio	Ti-Rich Side (nm)	Center (nm)	Al-Rich Side (nm)
90:10	91	71	86
80:20	63	41	84
70:30	92	87	130

Figure 2. SEM images of the thin films showing the surface grain clusters with varying Ar:N$_2$ gas ratios: (**a–c**) 90:10, (**d–f**) 80:20, and (**g–i**) 70:30, and different substrate locations.

3.2. Thickness

Table 3 shows the average thickness of the thin films in different Ar:N$_2$ gas ratios and positions. The measurements show that at higher partial Ar pressures at 90:10 N$_2$, the thickness of the film increases from the Ti-rich side to the Al-rich side. The variation in thickness is attributed to the difference in the sputtering yield of Al compared to that of Ti. That is, Al has a higher sputtering yield under bombardment with Ar or N ions leading to relatively thicker films on the Al-rich side.

Table 3. Average thickness of AlTiN thin films deposited at 90:10, 80:20, and 70:30 Ar:N$_2$ gas ratios measured using an optical laser scanner.

Ar:N$_2$ Ratio	Ti-Rich Side (nm)	Center (nm)	Al-Rich Side (nm)
90:10	550	550	930
80:20	130	200	110
70:30	1000	550	170

3.3. Energy-Dispersive X-ray Spectroscopy

Figure 3 shows the EDX linear scans of the thin films at different Ar:N$_2$ gas ratios. All profiles show increasing amounts of Ti content near the Ti-rich side, whereas increasing amounts of Al content can be observed near the Al-rich side. Furthermore, all the deposits obtained had high atomic percentages of Al that ranged from 60 to 70 at% compared to 29–40 at% for Ti, resulting in Al$_{0.60}$Ti$_{0.40}$N to Al$_{0.70}$Ti$_{0.30}$N stoichiometry.
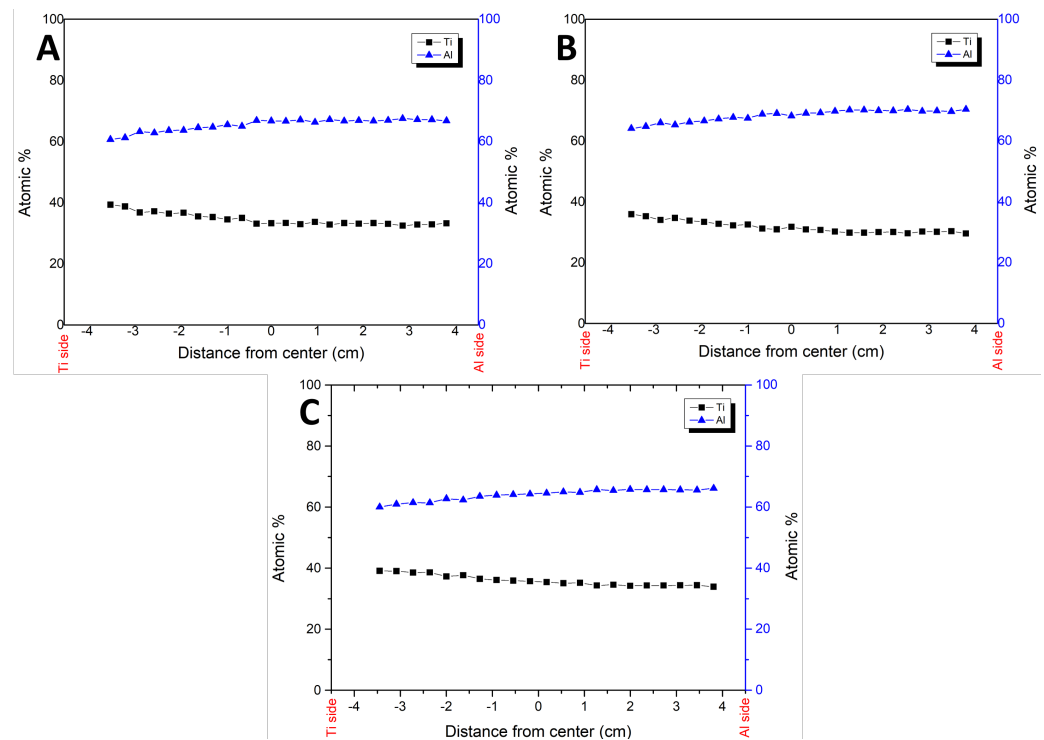
Figure 3. EDX line scan of the thin films at different Ar:N$_2$ gas ratios and substrate positions: (**A**) 70:30, (**B**) 80:20, (**C**) 90:10.

3.4. X-ray Diffraction

From the XRD of the samples shown in Figure 4 deposited using different gas ratios 90:10, 80:20, and 70:30, peaks around $2\theta = 44.56°$ and $2\theta = 74.63°$ correspond to face-centered cubic (FCC)-AlTiN peaks, while the peak at 50.6° corresponds to that of wurtzite-AlTiN (w-AlTiN). For all samples, the increase in w-AlTiN peak intensities with increasing Al content can be attributed to the preferential formation of wurtzite-AlN (w-AlN) at Al concentrations of 0.67 and higher.

3.5. Dynamic Microhardness

Table 4 summarizes the Vickers hardness values for the middle substrates at varying gas ratios. An increase in hardness was observed for Ar:N$_2$ gas ratios from 90:10 to 80:20, correlated with the decrease in grain size according to the SEM images (Figure 2). A one-way ANOVA was performed to determine the effect of the Ar:N$_2$ gas ratio on the hardness. There was a statistically significant difference in hardness between the three groups ($F(2,6) = 32.4$, $p = 6.07 \times 10^{-4}$). Tukey's honestly significant difference (HSD) test for multiple comparisons found that the mean value of the measured hardness was significantly different between all groups. The calculated HSD is 65 and the differences between all means (μ) of each group are greater than this value ($|\mu_{70:30} - \mu_{80:20}| = 170$, $|\mu_{80:20} - \mu_{90:10}| = 98$, $|\mu_{70:30} - \mu_{90:10}| = 71$). The thin films deposited in the center position of the stage showed well-defined indentation marks without cracking and delamination near the indentations.
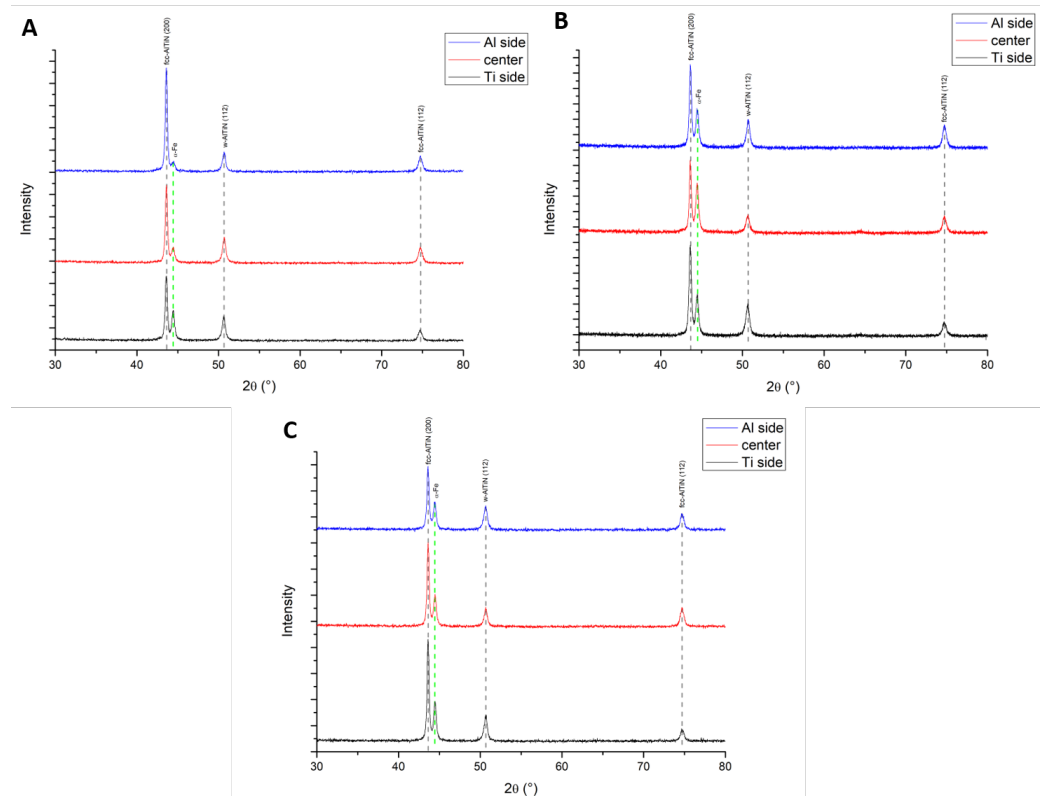
Figure 4. XRD pattern on varying Ar:N$_2$ gas ratios of (**A**) 70:30, (**B**) 80:20, and (**C**) 90:10.

Table 4. One-Way ANOVA for the measured hardness of middle substrates at varying Ar:N$_2$ gas ratios showing a statistically significant hardness of samples prepared with the 80:20 gas ratio.

Ar:N$_2$ Ratio	Count	Sum	Mean (HV)	Mean (GPa)	Variance	
70:30	3	1800	610	6.0	340	
80:20	3	2300	780	7.6	280	
90:10	3	2100	710	6.9	1400	
ANOVA Hardness (HV)						
Source of Variation	SS	df	MS	F	*p*-value	F crit
Between Groups	430	2.0	22,000	32	6.1×10^{-4}	5.1
Within Groups	4000	6.0	670			
Total	4700	8.0			HSD	65

4. Discussion

This work demonstrated a combinatorial approach to the growth of ternary nitride thin films. Using a two-half-disk target setup, variations in the composition of the film can be realized in a single experimental run by positioning the substrates at different locations on the sample stage. This approach would allow for the rapid evaluation of the deposited films and tailoring of the specific composition and properties by adjusting the deposition parameters. However, care must be taken to ensure that the target surface is free of contaminants prior to the start of the deposition process. Poisoning occurs as a result of the growth of compounds on the target surface as a result of reactions with the gas [18]. Target impurities caused by poisoning severely affect the sputtering process, including the deposition rate, stoichiometry, and film properties [19,20]. Target poisoning is commonly observed in DC reactive sputtering, such as the growth of TiN on Ti targets at high N$_2$ partial pressures [21]. In addition, targets such as Ti are also gettering materials, which could affect the partial pressure of the reactive gas, especially at high gas loads [22]. Thus,

in reactive sputtering processes, previously used targets should undergo target cleaning prior to deposition. The presputtering process can be achieved by running the discharge for a few minutes to remove unwanted layers on the target while the target shield is kept closed. Tuning the gas partial pressure ratios between reactive and inert gases is also important to minimize changes in the partial pressure ratios caused by the gettering effect of the target during the deposition process. Target contamination may occur in co-sputtering multitarget systems. This can be minimized by isolating the sputtering cathodes using target shields. The sputtering yield of each target can be tuned by adjusting the target bias, while the uniformity of the deposited films can be achieved by rotating the substrates. In the case of adjacent targets used in this study, since only one sputtering gun was used, the heavier atoms can lead to an increase in the sputtering yield of lighter atoms. This is because heavy atoms can act as backscattering centers for bombarding ions [23].

The SEM images revealed uniformly distributed grain sizes. The morphology is similar to the observations of Battiston et al. [24] and Szala et al. [25] where columnar growth was achieved. Furthermore, a decrease in the average grain size is observed when the N_2 content increases from 10% to 20%. However, grain agglomeration occurs when N_2 is around 20% or higher. The smallest grain size is measured at the central position of the 80:20 Ar:N_2.

The high Al content in all samples is attributed to the high sputtering yield of Al compared to Ti for incident Ar or N ions. These observations are supported by calculations using the empirical Yamamura sputtering yield formula [10]. As shown in Figure 5, Al sputtering yield is almost twice that of the Ti target for the incident ion energy range of 100 to 1000 eV. These observations are also supported by the atomic percentages seen in Tables 5 and 6.

Table 5. Atomic percentages of Ti in AlTiN films deposited at 90:10, 80:20, and 70:30 Ar:N_2 gas ratios.

Ar:N_2 Ratio	Ti Side (at%)	Center (at%)	Al Side (at%)
90:10	39	35	34
80:20	36	32	30
70:30	39	33	33

Table 6. Atomic percentages of Al in AlTiN films deposited at 90:10, 80:20, and 70:30 Ar:N_2 gas ratios.

Ar:N_2 Ratio	Ti Side (at%)	Center (at%)	Al Side (at%)
90:10	60	65	66
80:20	64	65	70
70:30	61	67	67

XRD results showed that FCC and wurtzite phases were the only phases of AlTiN obtained in this study in contrast to the metallic Ti, Al, TiN, and AlN peaks obtained by Li et al. [17] at different substrate positions. This may be due to having the half-disk target set-up where the ternary nitrides were formed. In the Li et al. [17] configuration, two separate Al and Ti sputtering targets were used that led to the formation of metallic films aside from the nitride films.

The thin film in the center position of the 80:20 Ar:N_2 gas ratio showed the highest average hardness measurement. The same sample had the smallest grain size as well, typical of the Hall-Petch effect as the grain sizes of the samples are still greater than the critical size of 10 nm [26]. Smaller grain sizes lead to an increase in hardness as a result of the accumulation of dislocations at the grain boundaries. This causes internal residual stresses, which increase the yield stress [27]. It is noteworthy, however, that all of the indentations were pre-set to the depth of 500 nm, and the film in the center position of the 80:20 Ar:N_2 gas ratio has a measured thickness of around 200 nanometers. This means that the substrate contributed to the majority of the measured hardness, with 304 SS having a lower hardness at less than 2.2 GPa [28,29].
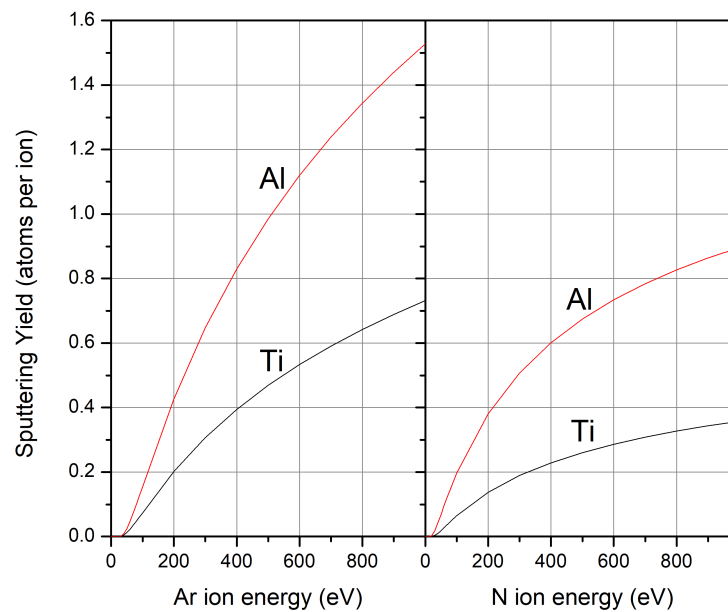
Figure 5. Sputtering yield calculations of Ti and Al targets under (**left**) Ar ion and (**right**) N ion bombardment.

The hardness of the resulting thin films was lower than the 33.9 GPa obtained by Fan et al. [30]. This can be attributed to the decrease in hardness with increasing Al content [31] starting at 60 at%. This also corresponds to the decrease in the FCC phases in the thin film and the increase in the amount of wurtzite phases, which contributes to a relatively softer film [32]. The absence of heating [7] and substrate bias [31], as well as having a relatively thin film, also contributed to the low hardness of the films. However, regardless of the gas ratio, the indentation marks did not exhibit cracking or delamination. This result indicates good film adhesion, similar to the observations of Vlassak et al. [33].

The growth of AlTiN thin films was achieved using this approach. Using only a single magnetron target configuration, the growth of multi-element films can be achieved by using sectors of a disk of different elements and assembling them to form a circular disk target, similar to putting together slices of a pizza. Adjusting the area of the target exposed to the energetic ions from the plasma allows one to control the amount of sputtered species of each element. This eventually allows control over the elemental composition of the deposited film. In this way, a single deposition run with multiple substrates placed at different locations with respect to the target can produce films with varying Al and Ti concentrations.

5. Conclusions

Thin films of AlTiN were successfully grown on 304 SS substrates via RF magnetron sputtering using Ar:N_2 ratios of 90:10, 80:20, and 70:30. This was achieved using a combinatorial process. EDX linear scan obtained a range of $Al_{0.60}Ti_{0.40}N$ to $Al_{0.70}Ti_{0.30}N$ for all runs, the high Al and low Ti contents obtained were attributed to their respective sputtering yield efficiencies and substrate location. XRD results confirm the presence of AlTiN with crystallographic peaks at 43.59° and 74.71° corresponding to the FCC-AlTiN peaks and 50.6° corresponding to the wurtzite phase of AlTiN, which increases with increasing Al content. SEM micrographs reveal nanometer-scale cauliflower-shaped grains with a corresponding decrease in grain size upon reaching the center of the substrates. From the 90:10 to 80:20 Ar:N_2 gas ratios, grain size refinement was observed before agglomeration from the 80:20 to 70:30 Ar:N_2 gas ratios. Hardness values of 6.0, 7.6, and 6.9 GPa were obtained from the center samples at runs with 90:10, 80:20, and 70:30 gas ratios, respectively. The highest value was achieved at the 80:20 sample, corresponding to the decrease in grain size at 80:20, attributed to the Hall-Petch effect. However, the softer 304 SS substrate with a

hardness of 2.2 GPa had a significant effect on the measured value since the indentation depth exceeded the film thickness. All samples exhibited good adhesion to 304 stainless steel substrates.

References

1. Bobzin, K. High-performance coatings for cutting tools. *CIRP J. Manuf. Sci. Technol.* **2017**, *18*, 1–9. [CrossRef]
2. Chang, Y.Y.; Chao, L.C. Effect of substrate bias voltage on the mechanical properties of AlTiN/CrTiSiN multilayer hard coatings. *Vacuum* **2021**, *190*, 110241. [CrossRef]
3. Zhang, Q.; Wu, Z.; Xu, Y.X.; Wang, Q.; Chen, L.; Kim, K.H. Improving the mechanical and anti-wear properties of AlTiN coatings by the hybrid arc and sputtering deposition. *Surf. Coat. Technol.* **2019**, *378*, 125022. [CrossRef]
4. Aihua, L.; Jianxin, D.; Haibing, C.; Yangyang, C.; Jun, Z. Friction and wear properties of TiN, TiAlN, AlTiN and CrAlN PVD nitride coatings. *Int. J. Refract. Met. Hard Mater.* **2012**, *31*, 82–88. [CrossRef]
5. Kawate, M.; Kimura Hashimoto, A.; Suzuki, T. Oxidation resistance of Cr1–XAlXN and Ti1–XAlXN films. *Surf. Coat. Technol.* **2003**, *165*, 163–167. [CrossRef]
6. Zhang, Q.; Xu, Y.; Zhang, T.; Wu, Z.; Wang, Q. Tribological properties, oxidation resistance and turning performance of AlTiN/AlCrSiN multilayer coatings by arc ion plating. *Surf. Coat. Technol.* **2018**, *356*, 1–10. [CrossRef]
7. García-González, L.; Garnica-Romo, M.G.; Hernández-Torres, J.; Espinoza-Beltrán, F.J. A study of TiAlN coatings prepared by rf co-sputtering. *Braz. J. Chem. Eng.* **2007**, *24*, 249–257. [CrossRef]
8. Rodríguez, R.; García, J.; Medrano, A.; Rico, M.; Sánchez, R.; Martínez, R.; Labrugère, C.; Lahaye, M.; Guette, A. Tribological behaviour of hard coatings deposited by arc-evaporation PVD. *Vacuum* **2002**, *67*, 559–566. [CrossRef]
9. Mo, J.; Zhu, M. Tribological oxidation behaviour of PVD hard coatings. *Tribol. Int.* **2009**, *42*, 1758–1764. [CrossRef]
10. Yamamura, Y.; Tawara, H. Energy dependence of ion-induced sputtering yields from monatomic solids at normal incidence. *At. Data Nucl. Data Tables* **1996**, *62*, 149–253. [CrossRef]
11. Yusof, A.S.; Hassan, Z. Characteristics of Cu-doped ZnO films prepared using magnetron co-sputtering. *J. Phys. Conf. Ser.* **2020**, *1535*, 012047. [CrossRef]
12. Liu, C.; Xu, J.; Liu, Z.; Ning, X.; Jiang, S.; Miao, D. Fabrication of highly electrically conductive Ti/Ag/Ti tri-layer and Ti–Ag alloy thin films on PET fabrics by multi-target magnetron sputtering. *J. Mater. Sci. Mater. Electron.* **2018**, *29*, 19578–19587. [CrossRef]
13. Hsu, S.Y.; Lai, Y.T.; Chang, S.Y.; Tsai, S.Y.; Duh, J.G. Combinatorial synthesis of reactively co-sputtered high entropy nitride (HfNbTiVZr)N coatings: Microstructure and mechanical properties. *Surf. Coat. Technol.* **2022**, *442*, 128564. [CrossRef]
14. Bikowski, A.; Siol, S.; Gu, J.; Holder, A.; Mangum, J.S.; Gorman, B.; Tumas, W.; Lany, S.; Zakutayev, A. Design of Metastable Tin Titanium Nitride Semiconductor Alloys. *Chem. Mater.* **2017**, *29*, 6511–6517. [CrossRef]
15. Greenaway, A.L.; Loutris, A.L.; Heinselman, K.N.; Melamed, C.L.; Schnepf, R.R.; Tellekamp, M.B.; Woods-Robinson, R.; Sherbondy, R.; Bardgett, D.; Bauers, S.; et al. Combinatorial Synthesis of Magnesium Tin Nitride Semiconductors. *J. Am. Chem. Soc.* **2020**, *142*, 8421–8430. [CrossRef] [PubMed]
16. Han, S.M.; Shah, R.; Banerjee, R.; Viswanathan, G.B.; Clemens, B.M.; Nix, W.D. Combinatorial studies of mechanical properties of Ti-Al thin films using nanoindentation. *Acta Mater.* **2005**, *53*, 2059–2067. [CrossRef]
17. Li, X.; Li, C.; Zhang, Y.; Tang, H.; Li, G.; Mo, C. Tribological properties of the Ti-Al-N thin films with different components fabricated by double-targeted co-sputtering. *Appl. Surf. Sci.* **2010**, *256*, 4272–4279. [CrossRef]
18. Arif, M.; Sauer, M.; Foelske-Schmitz, A.; Eisenmenger-Sittner, C. Characterization of aluminum and titanium nitride films prepared by reactive sputtering under different poisoning conditions of target. *J. Vacuum Sci. Technol. A* **2017**, *35*, 061507. [CrossRef]
19. Purandare, Y. P.; Ehiasarian, A. P.; Eh Hovsepian, P. Target poisoning during CrN deposition by mixed high power impulse magnetron sputtering and unbalanced magnetron sputtering technique. *J. Vacuum Sci. Technol. A* **2016**, *34*, 041502. [CrossRef]

20. Liu, L.; Li, W.; Sun, H.; Wang, G. Effects of Ti Target Purity and Microstructure on Deposition Rate, Microstructure and Properties of Ti Films. *Materials* **2022**, *15*, 2661. [CrossRef]

21. Nguyen, D.; Phan, Q.; Tran, D.; Pham, D. Effects of Ti Target Poisoning to Titanium Nitride Coating Fabricated by a Physical Vapor Deposition Technique. *Appl. Mech. Mater.* **2019**, *889*, 185–189. [CrossRef]

22. Depla, D.; De Gryse, R. Target poisoning during reactive magnetron sputtering: Part II: the influence of chemisorption and gettering. *Surf. Coat. Technol.* **2004**, *183*, 190–195. [CrossRef]

23. Volpian, O.D.; Kuzmichev, A.I.; Obod, Y.A. Change in ion sputtering coefficients of targets due to cross-dusting during simultaneous operation of two sputters. *J. Phys. Conf. Ser.* **2020**, *1713*, 012047. [CrossRef]

24. Battiston, S.; Montagner, F.; Fiameni, S.; Famengo, A.; Boldrini, S.; Ferrario, A.; Fanciulli, C.; Agresti, F.; Fabrizio, M. AlTiN based thin films for degradation protection of tetrahedrite thermoelectric material. *J. Alloys Compd.* **2019**, *792*, 953–959. [CrossRef]

25. Szala, M.; Walczak, M.; Pasierbiewicz, K.; Kamiński, M. Cavitation Erosion and Sliding Wear Mechanisms of AlTiN and TiAlN Films Deposited on Stainless Steel Substrate. *Coatings* **2019**, *9*, 340. [CrossRef]

26. Lumley, R.; Morton, A.; Polmear, I. Nanoengineering of metallic materials. In *Nanostructure Control of Materials*; Elsevier: Amsterdam, The Netherlands, 2006; pp. 219–250. [CrossRef]

27. Tan, C.; Kuang, T.; Zhou, K.; Zhu, H.; Deng, Y.; Li, X.; Cai, P.; Liu, Z. Fabrication and characterization of in-situ duplex plasma-treated nanocrystalline Ti/AlTiN coatings. *Ceram. Int.* **2016**, *42*, 10793–10800. [CrossRef]

28. Adler, T.A.; Walters, R.P. Wear and scratch hardness of 304 stainless steel investigated with a single scratch test. *Wear* **1993**, *162–164*, 713–720. [CrossRef]

29. Ge, S.; Wang, Y.; Song, W.; Ji, L.; Cai, L.; Zhang, Y. Preparation and characterization of a new type of 304 stainless steel metalocking key. *IOP Conf. Ser. Earth Environ. Sci.* **2019**, *358*, 052062. [CrossRef]

30. Fan, Q.X.; Wang, T.G.; Liu, Y.M.; Wu, Z.H.; Zhang, T.; Li, T.; Yang, Z.B. Microstructure and corrosion resistance of the AlTiN coating deposited by arc ion plating. *Acta Metall. Sin.* **2016**, *29*, 1119–1126. [CrossRef]

31. Andersson, J.; Vetter, J.; Müller, J.; Sjölén, J. Structural effects of energy input during growth of $Ti_{1-x}Al_xN$ ($0.55 \leqslant x \leqslant 0.66$) coatings by cathodic arc evaporation. *Surf. Coat. Technol.* **2014**, *240*, 211–220. [CrossRef]

32. Ravi, N.; Markandeya, R.; Joshi, S.V. Effect of nitrogen pressure on mechanical properties of nc-TiAlN/a-Si3N4 nanocomposite coatings deposited by cathodic arc PVD process. *Mater. Today Proc.* **2016**, *3*, 3002–3011. [CrossRef]

33. Vlassak, J.J.; Drory, M.D.; Nix, W.D. A simple technique for measuring the adhesion of brittle films to ductile substrates with application to diamond-coated titanium. *J. Mater. Res.* **1997**, *12*, 1900–1910. [CrossRef]